CHAPTER 5

Sliding Mode Control and FREN

From many computer experiments, it is found that the control system using two FRENs with parallel structure shown in the previous chapter sometimes becomes unstable. Since during the system operation, the plant information Y_p can become large when $\Delta u(k)$ is nearly zero. In this chapter, the direct adaptive controller based on the combination between FREN and the *Sliding Mode Control* (SMC) is proposed. The SMC is applied to estimate the upper and the lower bounds of the control signal to guarantee the system's stability. Within these bounds, the FREN controller generates a suitable control signal according to the given fuzzy control rules.

5.1 Estimation of Control Effort's Bounds

It is rather difficult to ensure the stability of FNN based adaptive control system because of its nonlinearity. In this work, the system stability condition is enforced by limiting the control signal to some pre-determined bounds. This stable control effort range is determined by using the modified SMC in the discrete-time domain.

Consider the general N-th order nonlinear discrete-time plant which can be written as

$$\begin{bmatrix} x_1(k+1) \\ x_2(k+1) \\ \vdots \\ x_{N-1}(k+1) \\ x_N(k+1) \end{bmatrix} = \begin{bmatrix} 0 & 1 & 0 & \cdots & 0 \\ 0 & 0 & 1 & \cdots & 0 \\ \vdots & & & \ddots & \vdots \\ 0 & 0 & & \cdots & 1 \\ 0 & 0 & 0 & \cdots & 0 \end{bmatrix} \begin{bmatrix} x_1(k) \\ x_2(k) \\ \vdots \\ x_{N-1}(k) \\ x_N(k) \end{bmatrix} + \begin{bmatrix} 0 \\ 0 \\ \vdots \\ 0 \\ g(\boldsymbol{x}(k)) \end{bmatrix} u(k) + \begin{bmatrix} 0 \\ 0 \\ \vdots \\ 0 \\ f(\boldsymbol{x}(k)) \end{bmatrix} + \begin{bmatrix} 0 \\ 0 \\ \vdots \\ 0 \\ d(k) \end{bmatrix}, \tag{5.1}$$

or more compactly as

$$\boldsymbol{x}(k+1) = \boldsymbol{A}\boldsymbol{x}(k) + \boldsymbol{B}_k u(k) + \boldsymbol{F}_k + \boldsymbol{D}_k, \tag{5.2}$$

here $f : \mathbb{R}^N \to \mathbb{R}$ and $g : \mathbb{R}^N \to \mathbb{R}$ are nonlinear functions. It is assumed that $\boldsymbol{x}(k)$ is finite for all k.

Define the sliding surface $s(k)$ as

$$s(k) = \boldsymbol{c}\Big[\boldsymbol{x}(k) - \boldsymbol{x}_d(k)\Big] = \boldsymbol{c}\boldsymbol{e}(k), \tag{5.3}$$

where $\boldsymbol{x}_d(k)$ be the desired value of $\boldsymbol{x}$ at time k and $\boldsymbol{c} = \begin{bmatrix} c_1 & \cdots & c_N \end{bmatrix}$ is a constant matrix. Note that $\boldsymbol{c}$ must not be orthogonal to $\boldsymbol{e}$. The selection of $\boldsymbol{c}$ is discussed in appendix A.1. Then $s(k+1)$ is

$$s(k+1) = \boldsymbol{c}\boldsymbol{A}\boldsymbol{x}(k) + \boldsymbol{c}\boldsymbol{B}_k u(k) + \boldsymbol{c}\boldsymbol{F}_k + \boldsymbol{c}\boldsymbol{D}_k - \boldsymbol{c}\boldsymbol{x}_d(k+1), \tag{5.4}$$

or

$$s(k+1) = \boldsymbol{c}_r\boldsymbol{x}(k) + c_N g_k u(k) + c_N q_k - \boldsymbol{c}\boldsymbol{x}_d(k+1), \tag{5.5}$$

where $\boldsymbol{c}_r = \begin{bmatrix} 0 & c_1 & \cdots & c_{N-1} \end{bmatrix}$, $g_k = g(\boldsymbol{x}(k))$, and $q_k = f(\boldsymbol{x}(k)) + d(k)$. Define the Lyapunov function

$$V(k) = s^2(k), \tag{5.6}$$

and

$$\begin{aligned} \Delta V(k) &= V(k+1) - V(k) \\ &= s^2(k+1) - s^2(k). \end{aligned} \tag{5.7}$$

For stability we must have $\Delta V(k) \leq 0$ which implies

$$\Big[s(k+1) + s(k)\Big]\Big[s(k+1) - s(k)\Big] \leq 0. \tag{5.8}$$

Assume that $|q_k| < \Phi_q$, $c_N > 0$ and $g_k > 0$. Define

$$\Lambda = \boldsymbol{c}\boldsymbol{x}_d(k+1) - \boldsymbol{c}_r\boldsymbol{x}(k). \tag{5.9}$$

Then consider the condition (5.8) in the following four cases.

Case I: $s(k+1) + s(k) > 0$ and $s(k+1) - s(k) < 0$
We obtain

$$-\Lambda + c_N g_k u(k) + c_N q_k + s(k) > 0, \tag{5.10}$$

$$-\Lambda + c_N g_k u(k) + c_N q_k - s(k) < 0. \tag{5.11}$$

These inequalities lead to

$$\frac{\Lambda - c_N q_k - s(k)}{c_N g_k} < u(k) < \frac{\Lambda - c_N q_k + s(k)}{c_N g_k}. \tag{5.12}$$

Define

$$u_{1p}(k) = \frac{\Lambda + c_N\Phi_q + s(k)}{c_N g_k} \quad (5.13)$$

$$> \frac{\Lambda - c_N q_k + s(k)}{c_N g_k}, \quad (5.14)$$

$$u_{1n}(k) = \frac{\Lambda - c_N\Phi_q - s(k)}{c_N g_k} \quad (5.15)$$

$$< \frac{\Lambda - c_N q_k - s(k)}{c_N g_k}. \quad (5.16)$$

Then we may conclude that

$$u_{1n}(k) < u(k) < u_{1p}(k). \quad (5.17)$$

It is required that $u_{1n}(k) < u_{1p}(k)$ which implies $s(k) > -c_N\Phi_q$.

Case II: $s(k+1) + s(k) < 0$ and $s(k+1) - s(k) > 0$
We obtain

$$-\Lambda + c_N g_k u(k) + c_N q_k + s(k) < 0, \quad (5.18)$$

$$-\Lambda + c_N g_k u(k) + c_N q_k - s(k) > 0, \quad (5.19)$$

which leads to

$$\frac{\Lambda - c_N q_k + s(k)}{c_N g_k} < u(k) < \frac{\Lambda - c_N q_k - s(k)}{c_N g_k}. \quad (5.20)$$

Define

$$u_{2p}(k) = \frac{\Lambda + c_N\Phi_q - s(k)}{c_N g_k}$$

$$> \frac{\Lambda - c_N q_k - s(k)}{c_N g_k},$$

$$u_{2n}(k) = \frac{\Lambda - c_N\Phi_q + s(k)}{c_N g_k}$$

$$< \frac{\Lambda - c_N q_k + s(k)}{c_N g_k}.$$

Again we may conclude that

$$u_{2n}(k) < u(k) < u_{2p}(k), \quad (5.21)$$

provide that $u_{2n}(k) < u_{2p}(k)$ which implies that $s(k) < c_N\Phi_q$.

Case III: $s(k+1) + s(k) = 0$
We obtain

$$-\Lambda + c_N g_k u(k) + c_N q_k + s(k) = 0, \quad (5.22)$$

thus

$$u(k) = \frac{\Lambda - c_N q_k - s(k)}{c_N g_k}, \tag{5.23}$$

From Eq.(5.23) we obtain

$$\frac{\Lambda - c_N \Phi_q - s(k)}{c_N g_k} < \frac{\Lambda - c_N q_k - s(k)}{c_N g_k} < \frac{\Lambda + c_N \Phi_q - s(k)}{c_N g_k},$$

or

$$u_{1n} < u(k) < u_{2p}. \tag{5.24}$$

It is required that $u_{2p}(k) > u_{1n}(k)$ which gives $c_N \Phi_q > 0$. This condition is always hold from the property of c_N and Φ_q.

Case IV: $s(k+1) - s(k) = 0$
We obtain

$$-\Lambda + c_N g_k u(k) + c_N q_k - s(k) = 0, \tag{5.25}$$

thus

$$u(k) = \frac{\Lambda - c_N q_k + s(k)}{c_N g_k}. \tag{5.26}$$

Again from Eq.(5.26), we obtain

$$\frac{\Lambda - c_N \Phi_q + s(k)}{c_N g_k} < \frac{\Lambda - c_N q_k + s(k)}{c_N g_k} < \frac{\Lambda + c_N \Phi_q + s(k)}{c_N g_k},$$

or

$$u_{2n} < u(k) < u_{1p}. \tag{5.27}$$

It is required that $u_{1p}(k) > u_{2n}(k)$ which implies $c_N \Phi_q > 0$. This condition is always hold from the property of c_N and Φ_q.

Finally, the four conditions are summarized in Table 5.1. In this work, the control effort obtained from FREN controller is kept within the boundary obtained from SMC. This combination yields satisfactory results as shown in the next section.

5.2 FREN with SMC Controller

When using the proposed FREN as a controller, the structure of the control system becomes as shown in Fig. 5.1. The FREN receives the error signal $E(k)$ and computes the control signal $u(k)$. The plant control signal $u(k)$ is obtained from

$$u(k) = O(k), \tag{5.28}$$

Table 5.1: Stable bound of control effort obtained from SMC.

Case	Bound of Control Effort	Sliding Surface Condition
I	$u_{1n} < u(k) < u_{1p}$	$s(k) > -c_N \Phi_q$
II	$u_{2n} < u(k) < u_{2p}$	$s(k) < c_N \Phi_q$
III	$u_{1n} < u(k) < u_{2p}$	-
IV	$u_{2n} < u(k) < u_{1p}$	-

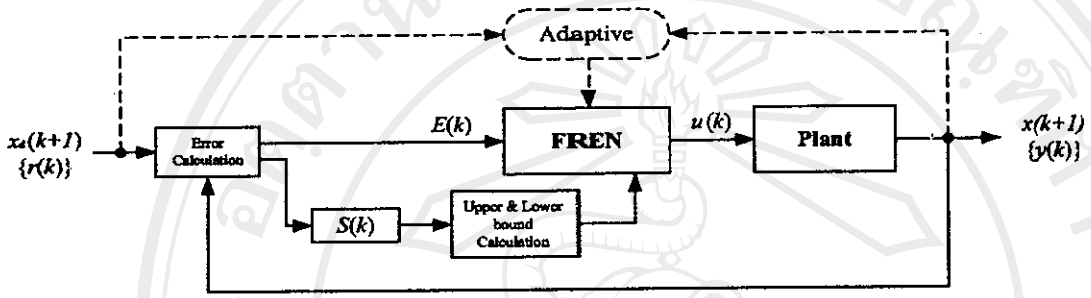

Figure 5.1: Control system using FREN and SMC

where $O(k)$ is the output of FREN in Eq.(3.3).

As an example of how the initial value of FREN's parameters are selected, consider the following 4 fuzzy control rules,

RULE 1 IF E IS PL THEN u IS PL
RULE 2 IF E IS PM THEN u IS PM
RULE 3 IF E IS NM THEN u IS NM
RULE 4 IF E IS NL THEN u IS NL.

Assume that the error signal $E \in [-1, 1]$ and the calculated lower and upper bound of the control effort obtained from SMC are -2 and 2, respectively, i.e. $u_k \in [-2, 2]$. The value of the control effort, u_k can be set by parameters in LC (e.g. h_i and k_i for $i = 1, 2, 3, 4$.) In this example, h_1 is set to the upper bound ($h_1 = 2$) and h_4 is set to the lower bound ($h_4 = -2$). The other parameters are $h_2 = \frac{h_1}{2} = 1$, $h_3 = \frac{h_4}{2} = -1$, and $k_i = 0$ for $i = 1, 2, 3, 4$. Then, MF parameters are

selected to cover the error range. The initial setting of all parameters are given as:

$$\text{Rule 1}: \quad A_1 = \mu_1(E) = \frac{1}{1+\exp\left[-20(E-0.35)\right]} \quad ; B_1 = 2A_1,$$

$$\text{Rule 2}: \quad A_2 = \mu_2(E) = \exp\left(-\left[\frac{E-0.25}{0.15}\right]^2\right) \quad ; B_2 = A_2,$$

$$\text{Rule 3}: \quad A_3 = \mu_3(E) = \exp\left(-\left[\frac{E+0.25}{0.15}\right]^2\right) \quad ; B_3 = -A_3,$$

$$\text{Rule 4}: \quad A_4 = \mu_4(E) = \frac{1}{1+\exp\left[20(E+0.35)\right]} \quad ; B_4 = -2A_4.$$

The results of this setting are shown in Fig. 5.2.

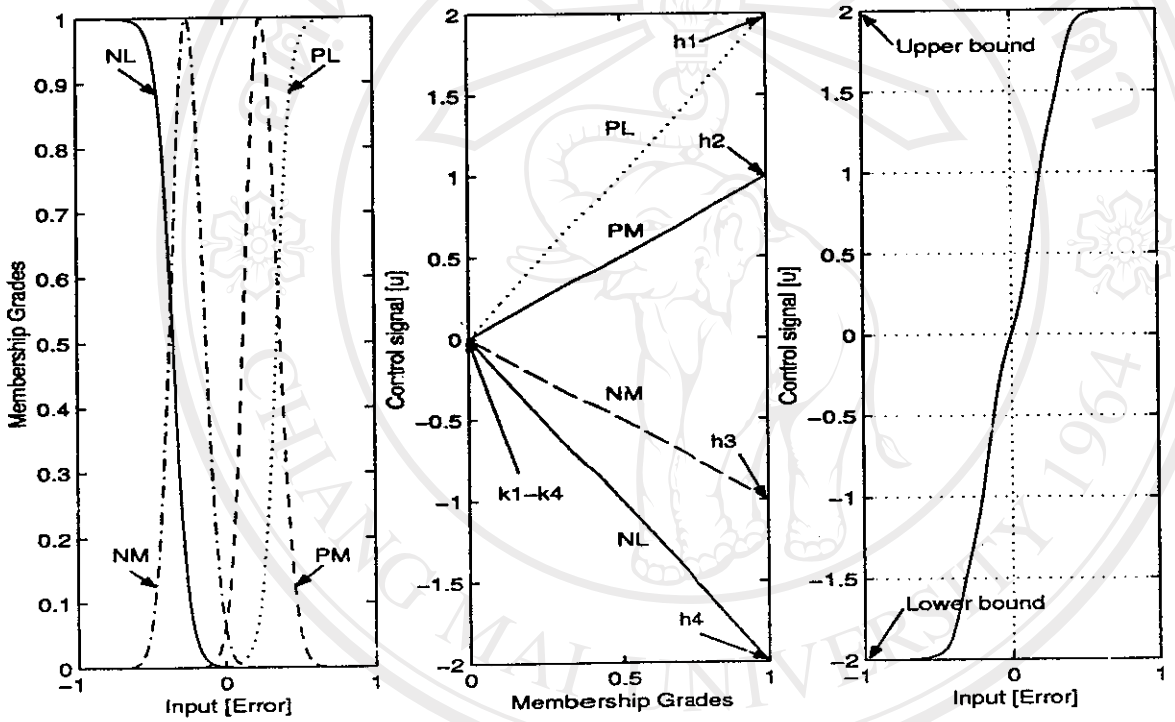

Figure 5.2: FREN parameters setting

5.3 Computer Simulation Examples

The performance of the proposed controller are tested by controlling some nonlinear plants. Some examples are presented in this section.

5.3.1 Robotic Control

The characteristic of the nonlinear discrete-time robotic plant [50] is

$$y(k+1) = (2T-1)y(k-1)+2(1-T)y(k)+10T^2\sin(y(k-1))+u(k)+d(k), \quad (5.29)$$

or in state equations form as

$$\begin{bmatrix} x_1(k+1) \\ x_2(k+1) \end{bmatrix} = \begin{bmatrix} 0 & 1 \\ 0 & 0 \end{bmatrix} \begin{bmatrix} x_1(k) \\ x_2(k) \end{bmatrix} + \begin{bmatrix} 0 \\ f(\boldsymbol{x}(k)) \end{bmatrix} + \begin{bmatrix} 0 \\ u(k) \end{bmatrix} + \begin{bmatrix} 0 \\ d(k) \end{bmatrix}, \tag{5.30}$$

where $x_2(k) = y(k)$, $x_1(k) = y(k-1)$, $u(k)$ is the control signal, T is the sampling interval and equals to 0.01 second, $d(k)$ is the external disturbance and

$$f(\boldsymbol{x}(k)) = (2T-1)x_1(k) + 2(1-T)x_2(k) + 10T^2 \sin(x_1(k)).$$

The reference signal y_d is set as

$$y_d(k+1) = \frac{\pi}{2} \sin\left(\frac{\pi}{5} kT\right). \tag{5.31}$$

Then $\boldsymbol{x}_d$ can be written as

$$\boldsymbol{x}_d(k+1) = \begin{bmatrix} x_{d1}(k+1) \\ x_{d2}(k+1) \end{bmatrix} = \frac{\pi}{2} \begin{bmatrix} \sin\left(\frac{\pi}{5} kT\right) \\ \sin\left(\frac{\pi}{5}(k+1)T\right) \end{bmatrix}. \tag{5.32}$$

The external disturbance is assumed to be

$$d(k) = \Phi_d \Gamma, \tag{5.33}$$

where $\Phi_d = 0.6$ and Γ is a uniformly distributed random number in $[-1, 1]$.

Let y_{max} be the maximum value of $y(k)$, then from the uncontrolled system response of Eq.(5.29) it is found that

$$y_{max} \approx 1.8, \tag{5.34}$$

where $d(k) = 0$. $\boldsymbol{c}$ in Eq.(5.3) is defined as $\boldsymbol{c} = \begin{bmatrix} 1 & 2 \end{bmatrix}$.

Denote the error $E = y_d - y$ and the fuzzy control rules are given by,

RULE 1 IF E IS PL THEN u IS PL
RULE 2 IF E IS PM THEN u IS PM
RULE 3 IF E IS NM THEN u IS NM
RULE 4 IF E IS NL THEN u IS NL,

In this simulation, the initial setting of membership functions and linear consequences of FREN are selected as shown in Fig. 5.3(a). After on-line learning, the final MF and LC of FREN become as shown in Fig. 5.3(b).

The initial output signal $y(k)$, the control effort $u(k)$, the output state error $e(k) = x_2(k) - x_{d2}(k)$ and the disturbance $d(k)$ are shown in Fig. 5.4(a)-(d), respectively. The on-line learning is applied around 1,000 epochs and the final results are obtained as shown in Fig. 5.5.

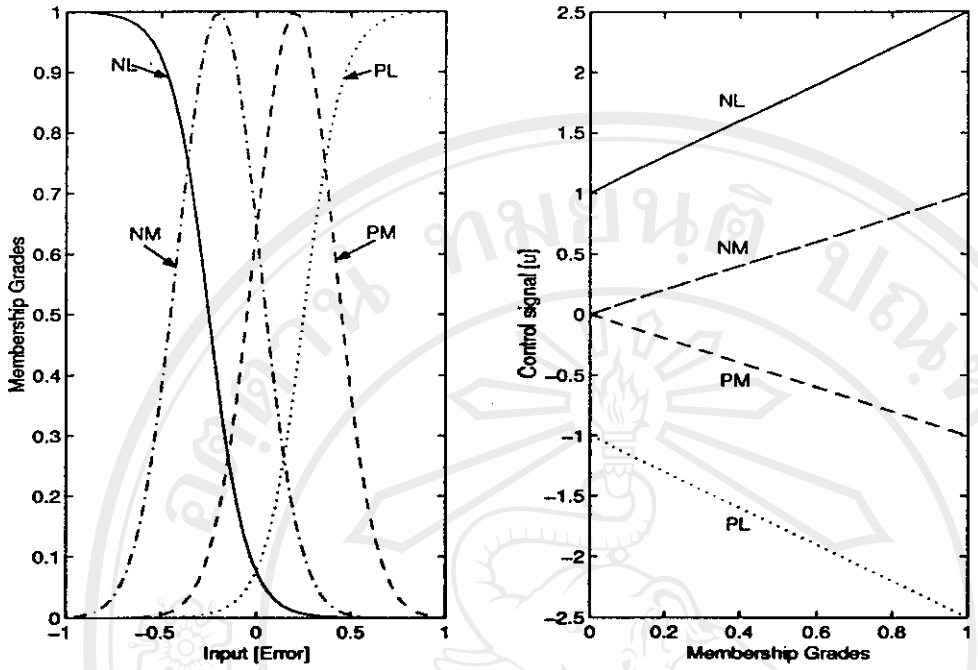

(a) Initial setting

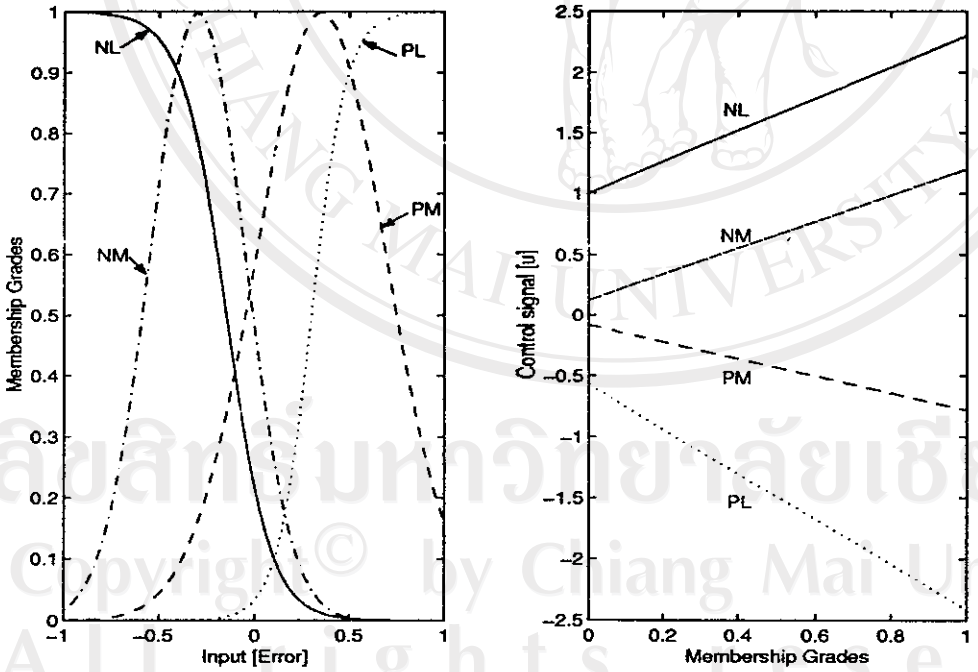

(b) Final setting

Figure 5.3: MF and LC for robotic control system.

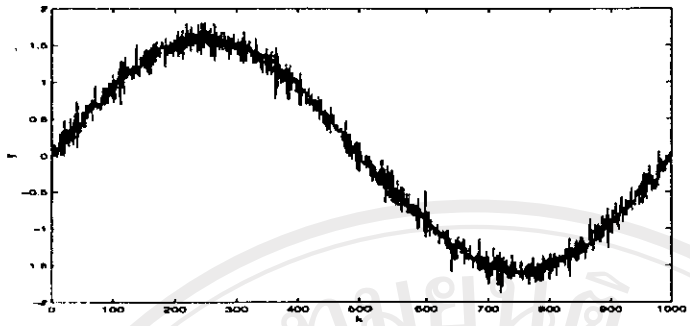

(a) Output $y(k)$.

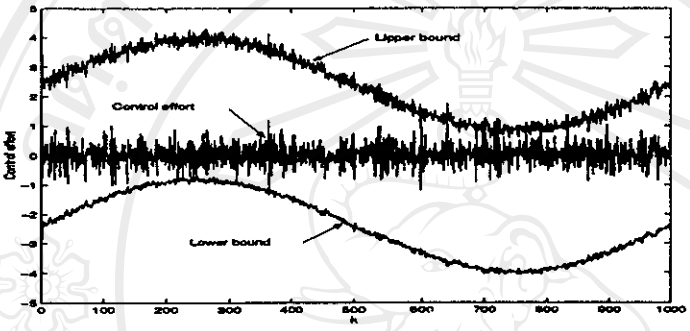

(b) Control effort $u(k)$ and its bounds.

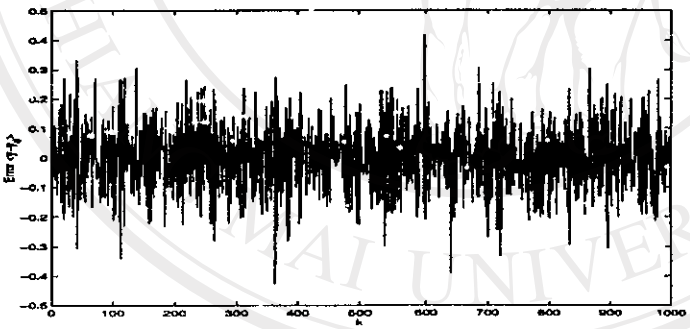

(c) Error $e(k)$.

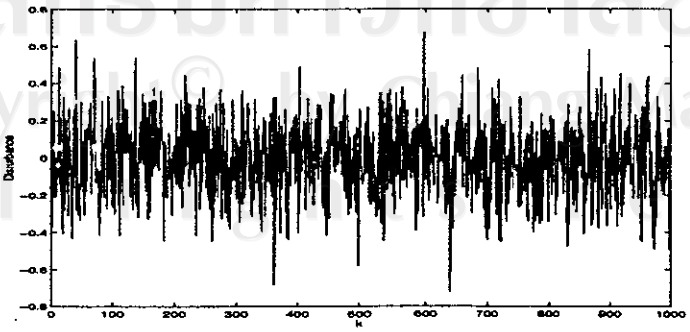

(d) Disturbance $d(k)$.

Figure 5.4: *Initial* simulation results of robotic control.

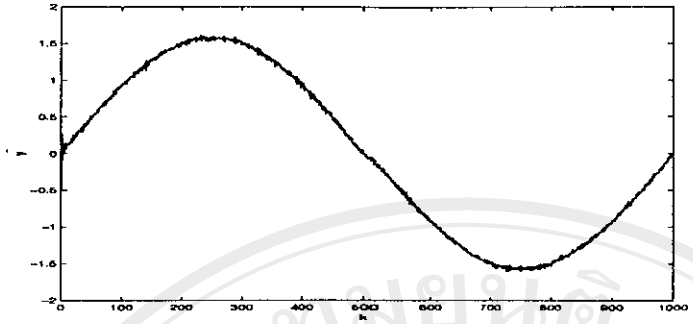

(a) Output $y(k)$.

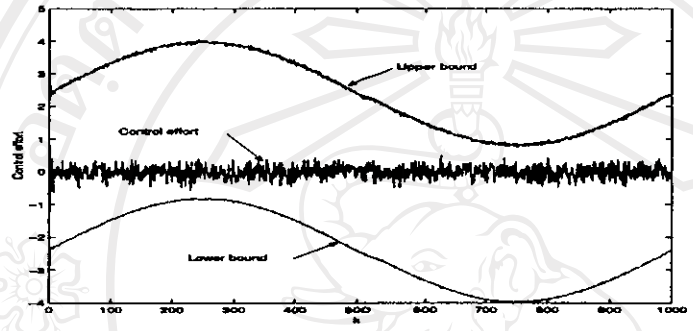

(b) Control effort $u(k)$ and its bounds.

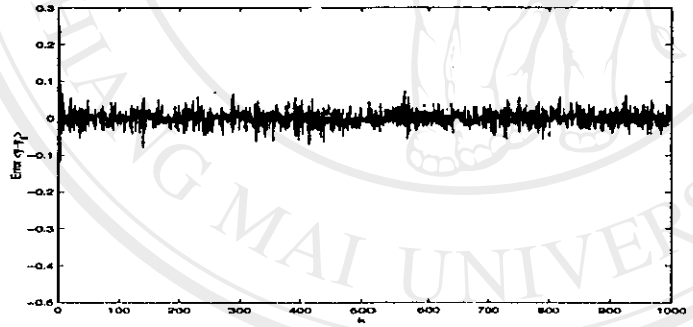

(c) Error $e(k)$.

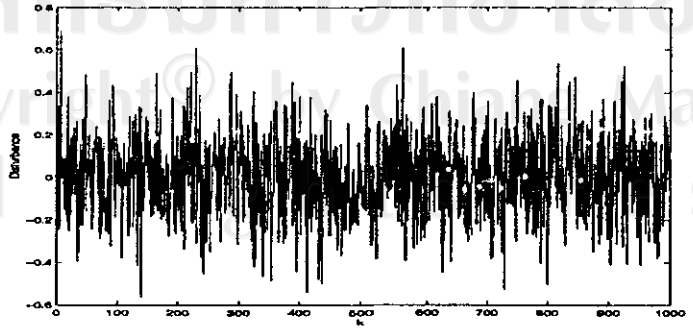

(d) Disturbance $d(k)$.

Figure 5.5: *Final* simulation results of robotic control.

5.3.2 Chaotic System Control

5.3.2.1 Heńon Map

The characteristic of the controlled nonlinear discrete-time Hénon map [12,21] is

$$y(k+1) = A + u(k) - y^2(k) + By(k-1), \tag{5.35}$$

where $A = 1.29$, $B = 0.3$. In state equation form, Eq.(5.35) becomes

$$\begin{bmatrix} x_1(k+1) \\ x_2(k+1) \end{bmatrix} = \begin{bmatrix} 0 & 1 \\ 0 & 0 \end{bmatrix} \begin{bmatrix} x_1(k) \\ x_2(k) \end{bmatrix} + \begin{bmatrix} 0 \\ f(\boldsymbol{x}(k)) \end{bmatrix} + \begin{bmatrix} 0 \\ g(\boldsymbol{x}(k)) \end{bmatrix} u(k), \tag{5.36}$$

where $x_2(k) = y(k)$, $x_1(k) = y(k-1)$, $u(k)$ is the control signal, $g(\boldsymbol{x}(k)) = 1$ and

$$f(\boldsymbol{x}(k)) = A - x_2^2(k) + Bx_1(k). \tag{5.37}$$

Let $\boldsymbol{c} = \begin{bmatrix} 1 & 2 \end{bmatrix}$. The chaotic state trajectory without the control effort ($u(k) = 0$) is shown in Fig 5.6.

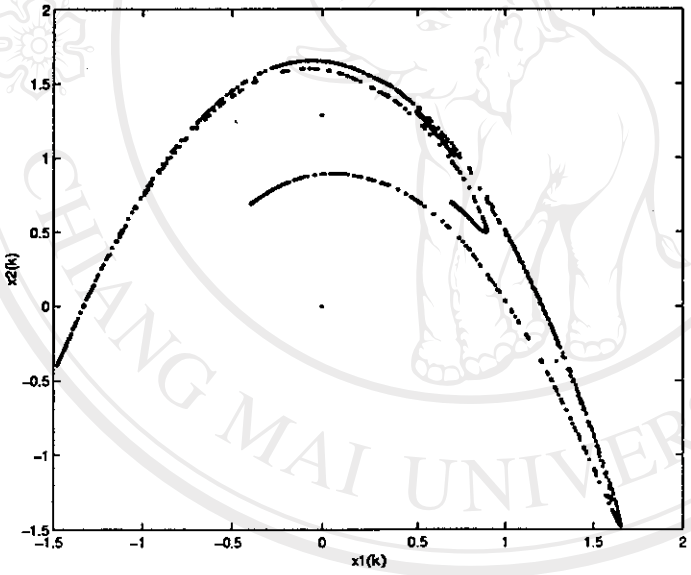

Figure 5.6: State trajectory of Hénon map.

The fixed point y_F is set to 0.838486. Then $\boldsymbol{x}_d$ can be written as

$$\boldsymbol{x}_d(k+1) = \begin{bmatrix} x_{d1}(k+1) \\ x_{d2}(k+1) \end{bmatrix} = \begin{bmatrix} y_F \\ y_F \end{bmatrix}. \tag{5.38}$$

Denoting the error $E = y_F - y$, the fuzzy control rules are given by,

RULE 1 IF E IS PL THEN u IS PL
RULE 2 IF E IS PM THEN u IS PM
RULE 3 IF E IS NM THEN u IS NM
RULE 4 IF E IS NL THEN u IS NL.

In this simulation, the controller starts to generate control effort at $k = 200$ and stops at $k = 800$. The initial setting of membership functions and linear consequences of FREN are selected as shown in Fig. 5.7(a). After on-line learning, the final MF and LC of FREN are shown in Fig. 5.7(b).

The initial output signal $y(k)$, control effort $u(k)$ and output state error $e(k) = x_2(k) - x_{d2}(k)$ are presented in Fig. 5.8(a)-(c), respectively. After that, the on-line learning is applied around 2000 epochs. The final results are shown in Fig. 5.9.

Next, the desired strategy is changed to

$$\boldsymbol{x}_d(k+1) = \frac{\pi}{2}\begin{bmatrix} \sin(0.01\frac{\pi}{1.5}k) \\ \sin(0.01\frac{\pi}{1.5}(k+1)) \end{bmatrix}. \tag{5.39}$$

The results are obtained as shown in Fig. 5.10. The relation between the control effort and its bounds can be noticed.

In order to investigate the effect of SMC bounds on the system's stability, another computer experiment is performed. In this test the control effort is allowed to lie outside the stability bounds at $k = 400$ to $k = 450$. During these time steps, as can be noticed in Fig.5.11, the output $y(k)$ cannot follow the desired trajectory. When the control effort is forced to be within the sliding bounds again after $k = 450$, the good tracking performance is obtained.

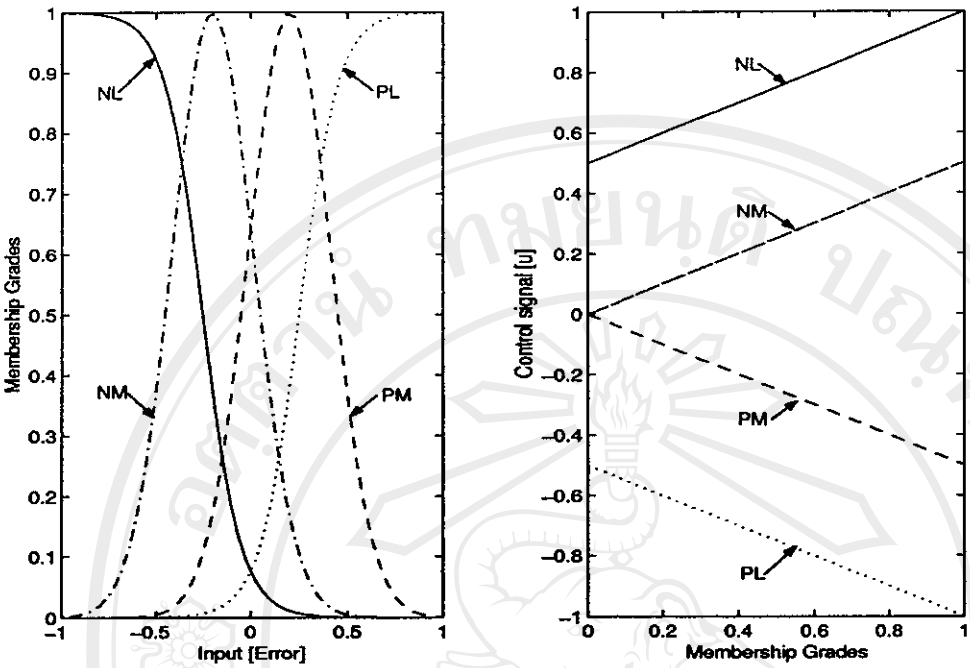

(a) Initial setting.

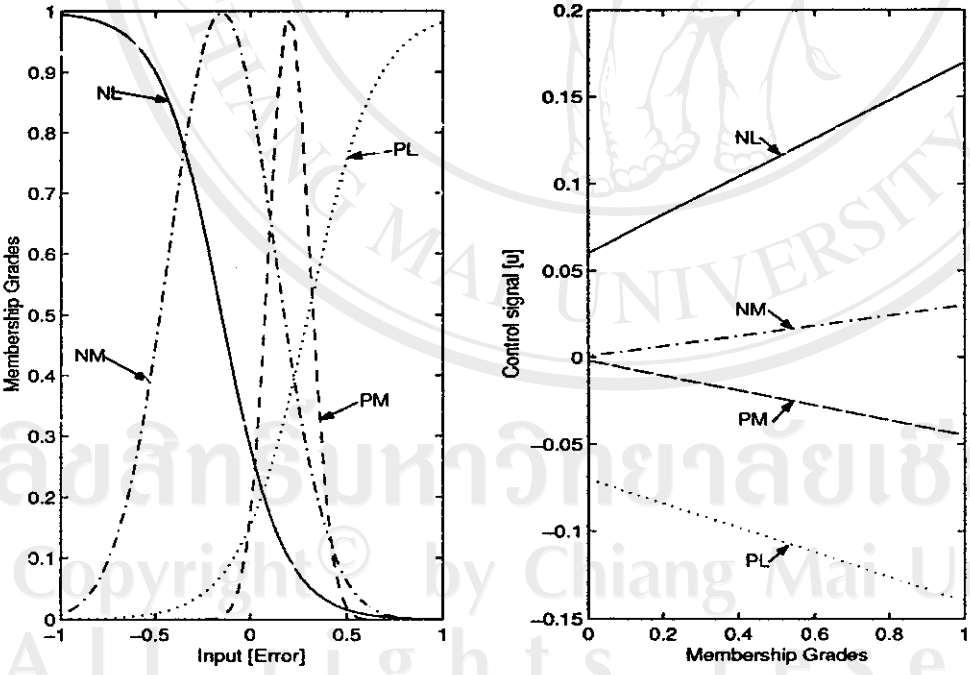

(b) Final setting.

Figure 5.7: MF and LC for Hénon map control.

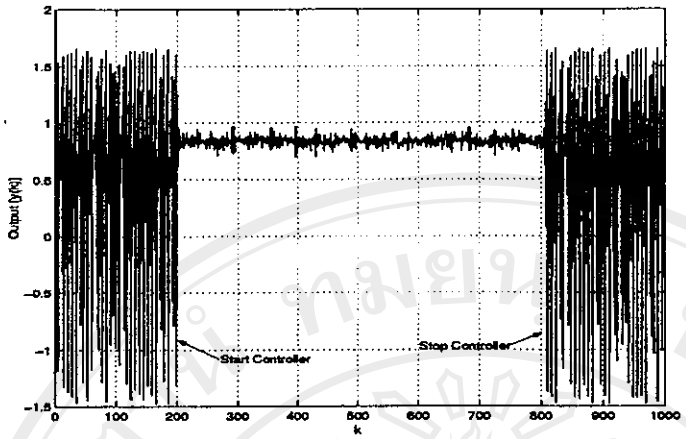

(a) Output $y(k)$.

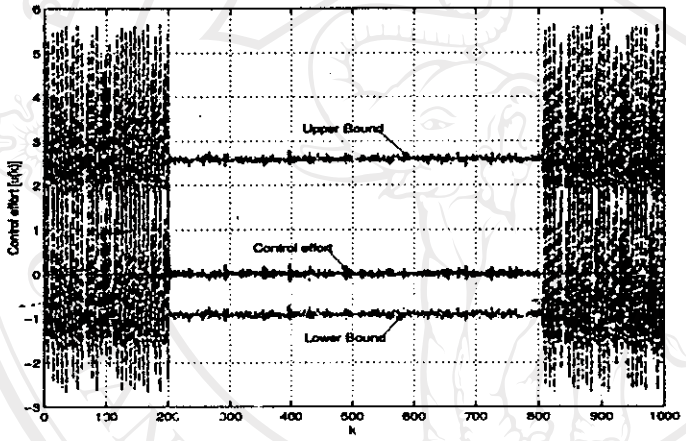

(b) Control effort $u(k)$ and its bounds.

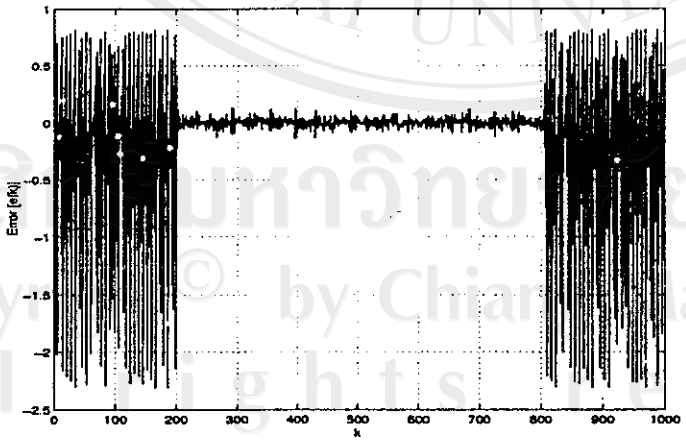

(c) Error $e(k)$.

Figure 5.8: *Initial* simulation results of Hénon map control.

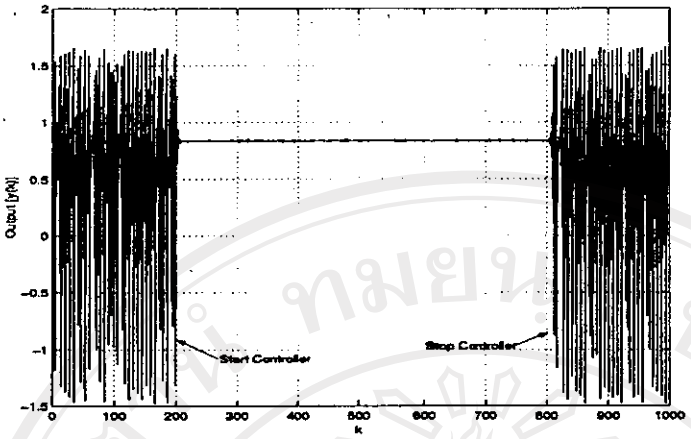

(a) Output $y(k)$.

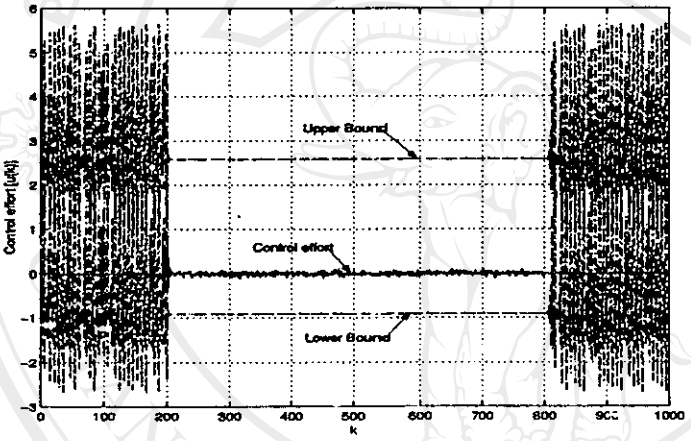

(b) Control effort $u(k)$ and its bounds.

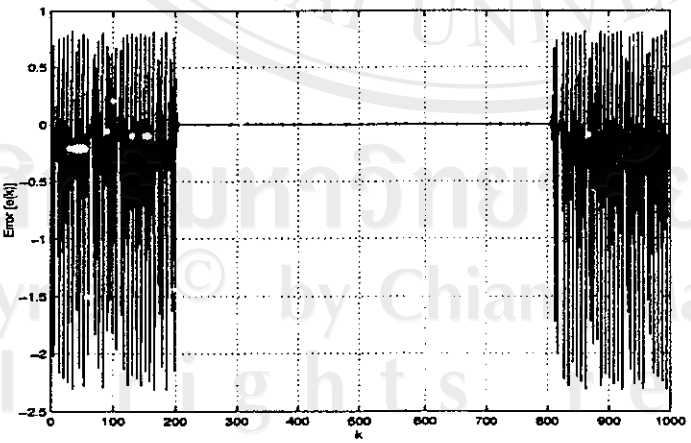

(c) Error $e(k)$.

Figure 5.9: *Final* simulation results of Hénon map control.

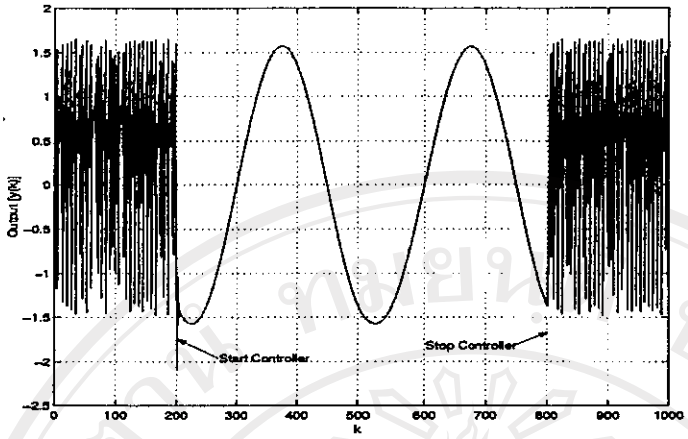

(a) Output $y(k)$.

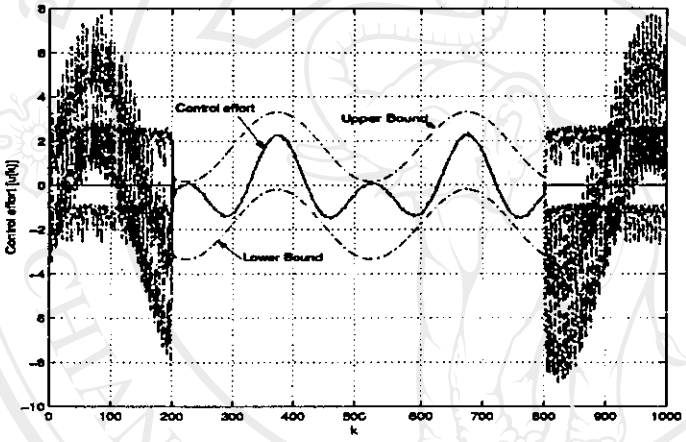

(b) Control effort $u(k)$ and its bounds.

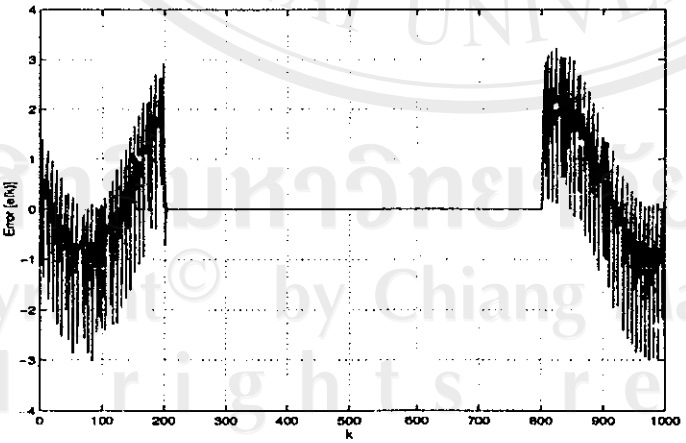

(c) Error $e(k)$.

Figure 5.10: Simulation results of Hénon map control when $\boldsymbol{x}_d$ is sine waveform.

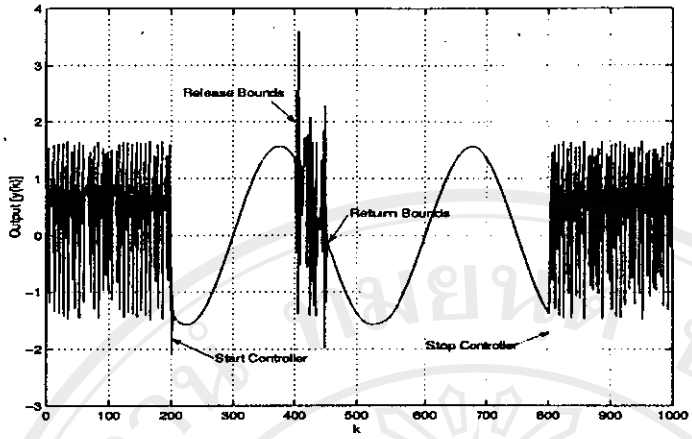

(a) Output $y(k)$.

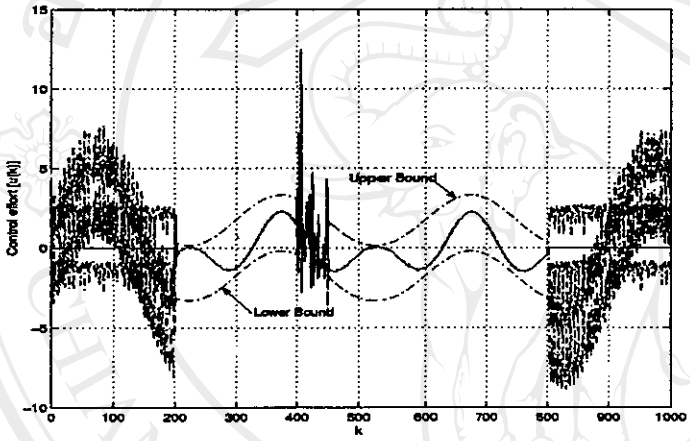

(b) Control effort $u(k)$ and its bounds.

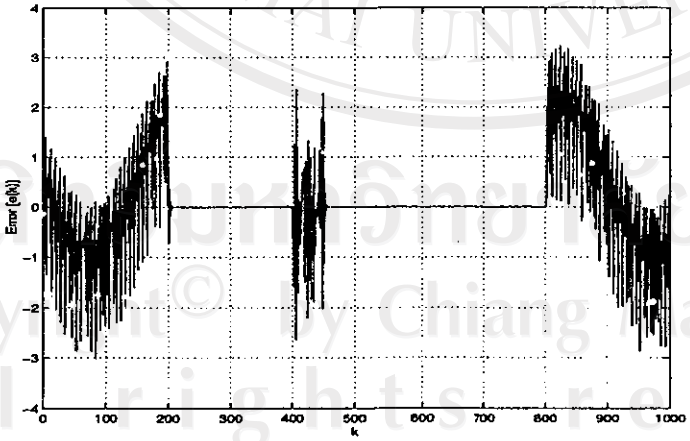

(c) Error $e(k)$.

Figure 5.11: Simulation results of Hénon map control when x_d is sine waveform and stable bounds are released.

5.3.2.2 Logistic Map

Here the proposed controller is used to control the logistic map [18, 62] whose nonlinear discrete-time equation is given by

$$y(k+1) = \Big(p + u(k)\Big)\, y(k) \Big(1 - y(k)\Big), \tag{5.40}$$

where $p = 3.79$. This can be rewritten as

$$\begin{bmatrix} x_1(k+1) \\ x_2(k+1) \end{bmatrix} = \begin{bmatrix} 0 & 1 \\ 0 & 0 \end{bmatrix} \begin{bmatrix} x_1(k) \\ x_2(k) \end{bmatrix} + \begin{bmatrix} 0 \\ f(\boldsymbol{x}(k)) \end{bmatrix} + \begin{bmatrix} 0 \\ g(\boldsymbol{x}(k)) \end{bmatrix} u(k), \tag{5.41}$$

where $x_2(k) = y(k)$, $x_1(k) = y(k-1)$, $u(k)$ is the control signal,

$$g(\boldsymbol{x}(k)) = x_2(k) - x_2^2(k), \tag{5.42}$$

and

$$f(\boldsymbol{x}(k)) = p x_2(k)[1 - x_2(k)]. \tag{5.43}$$

And $\boldsymbol{c} = \begin{bmatrix} 1 & 2 \end{bmatrix}$ which is the same as used in the previous example. The chaotic state trajectory is shown in Fig 5.12.

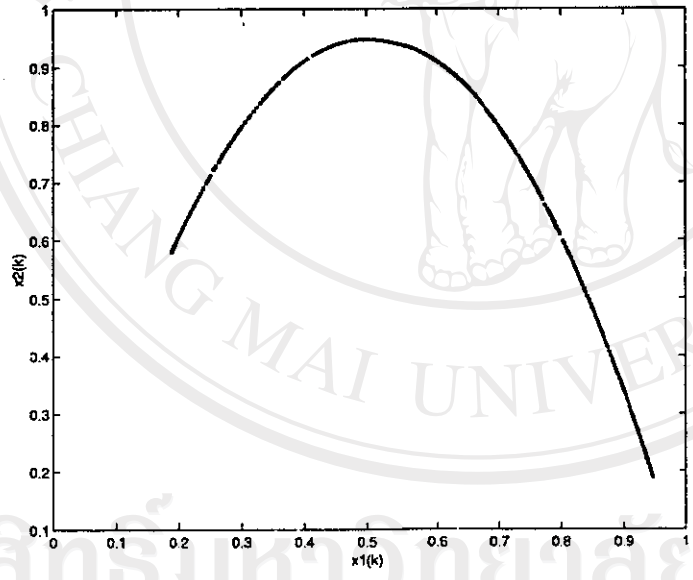

Figure 5.12: State trajectory of logistic map.

The fixed point y_F of $\boldsymbol{x}_d$ in (5.38) is set to 0.736148. Denote the error $E = y_F - y$, the fuzzy control rules are given by,

RULE 1 IF E IS PL THEN u IS PL
RULE 2 IF E IS PM THEN u IS PM
RULE 3 IF E IS NM THEN u IS NM
RULE 4 IF E IS NL THEN u IS NL,

Table 5.2: Comparison of Logistic map control.

Control algorithm	SSE	Training (epoch)	Adjustable parameters
OGY [14] method	1.139	-	-
Neural Network [1:4:1]	Fail	5,000	13
Neural Network [1:50:1]	1.025	2,000	151
RBF[1:4:1]	Fail	5,000	16
RBF[1:50:1]	0.8196	2,000	200
ANFIS[1:20:1]	0.2473	2,000	80
ANFIS[1:4:1]	0.5127	2,000	16
FREN [1:4:1]	0.2344	2,000	16

Note that SSE $= \sum_{k=201}^{800} e^2(k)$, and [X:Y:Z] denote the number of nodes in the input, the hidden and the output layer respectively.

The initial setting of membership functions and linear consequences of FREN are selected as shown in Fig. 5.13(a). After on-line learning, the final MF and LC of FREN become as shown in Fig. 5.13(b).

The initial output signal $y(k)$, control effort $u(k)$ and output state error $e(k) = x_2(k) - x_{d2}(k)$ are represented in Fig. 5.14(a)-(c), respectively. After that, the on-line learning is applied around 2000 epochs. The final result is shown in Fig. 5.15. Controlling of the logistic map by using other techniques are also performed and the results are summarized in Table 5.2.

It is found that using the neural network and the RBF with 4 hidden nodes cannot drive the system to reach the desired trajectory. The results obtained from FREN[1:4:1] and ANFIS[1:20:1] are similar. However, the number of adjustable parameters of ANFIS is around 5 times of FREN's.

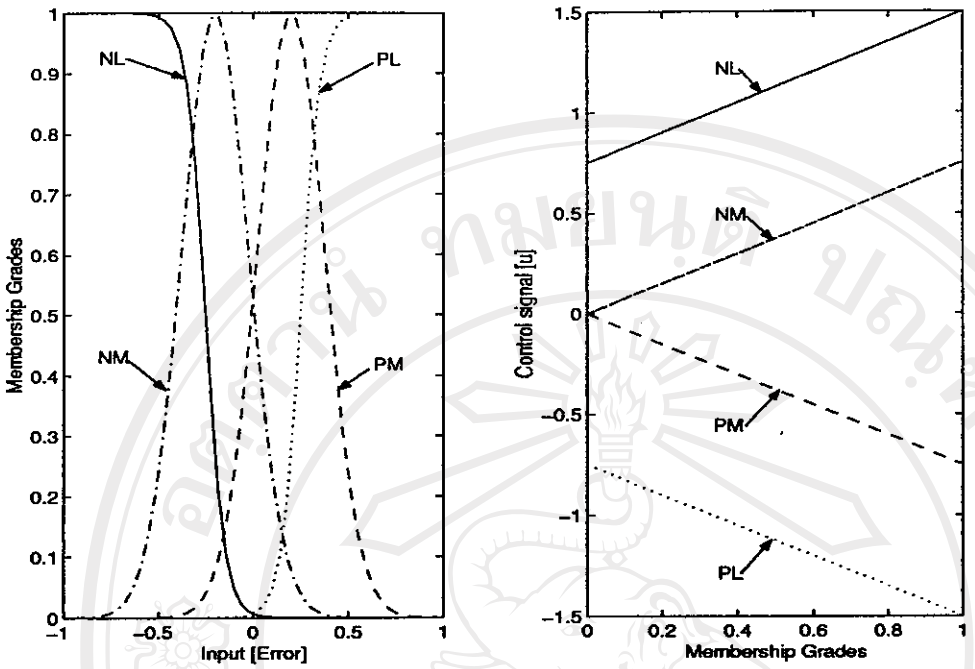

(a) Initial setting.

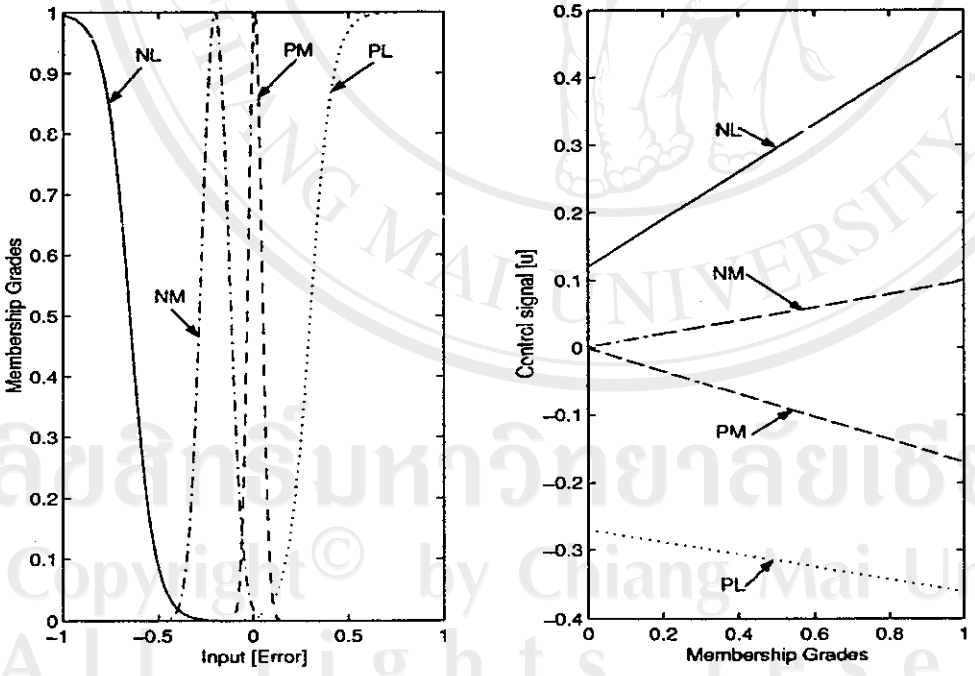

(b) Final setting.

Figure 5.13: MF and LC for logistic map control.

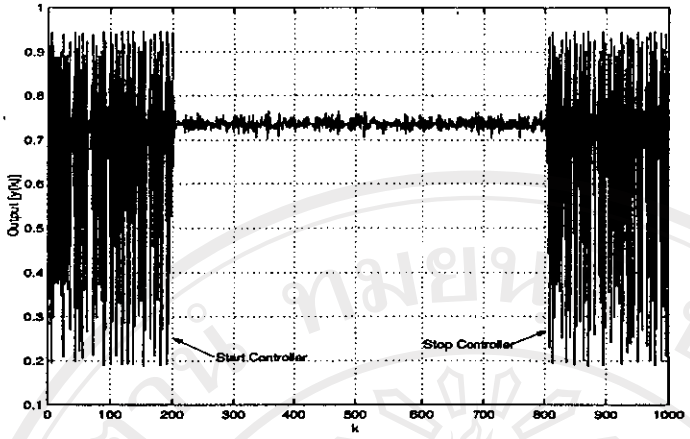

(a) Output $y(k)$.

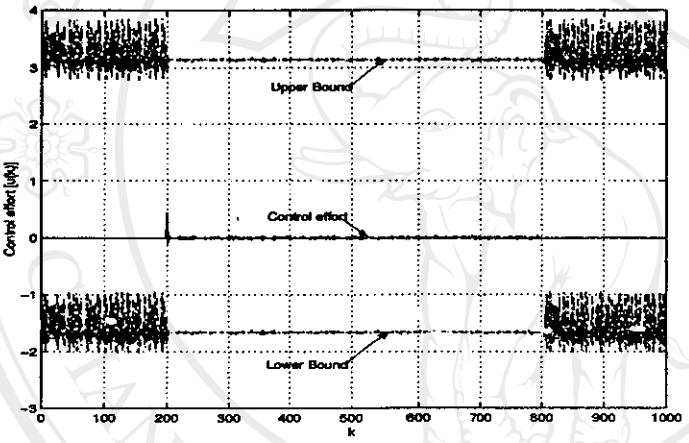

(b) Control effort $u(k)$ and its bounds.

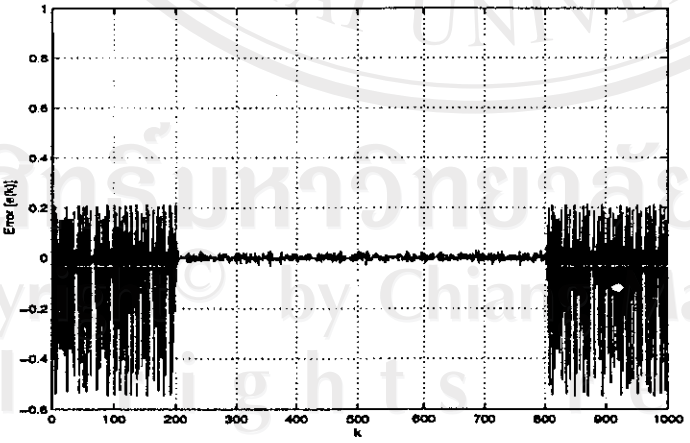

(c) Error $e(k)$.

Figure 5.14: *Initial* simulation results of logistic map control.

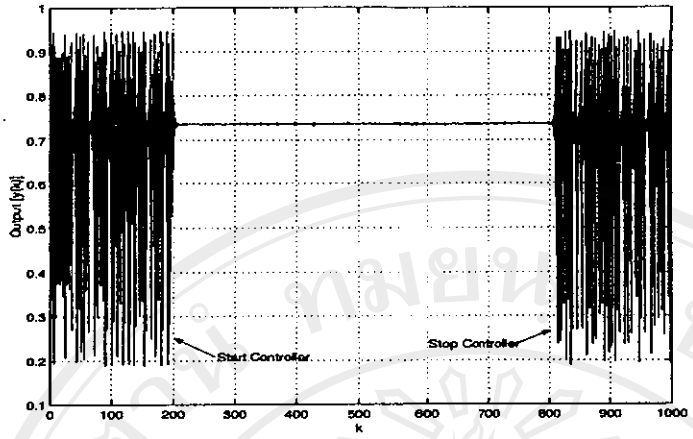

(a) Output $y(k)$.

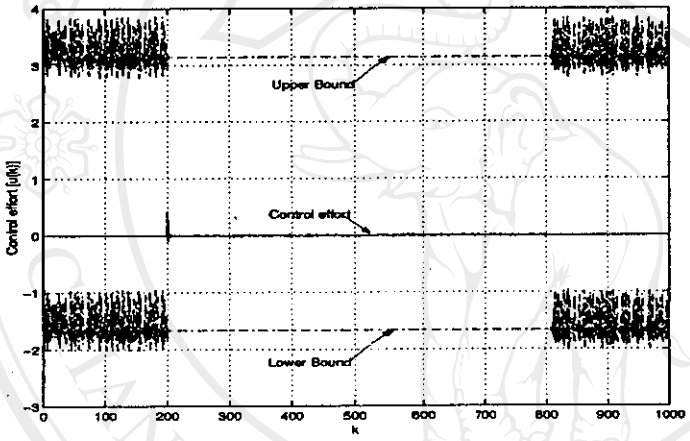

(b) Control effort $u(k)$ and its bounds.

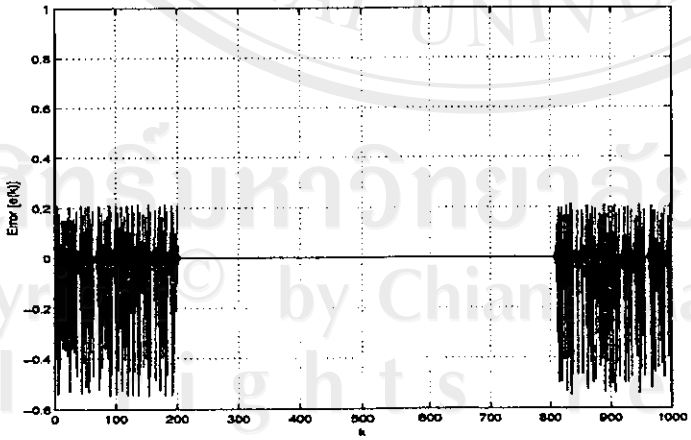

(c) Error $e(k)$.

Figure 5.15: *Final* simulation results of logistic map control.

5.3.3 Chaotic Synchronization

In this example, the FREN are applied to the 3-dimensional Hénon map synchronization [36, 40, 59] application. The characteristic of the 3-dimensional discrete-time Hénon map is

$$\begin{aligned} x_{1d}(k+1) &= -bx_{3d}(k) \\ x_{2d}(k+1) &= x_{1d}(k) + bx_{3d}(k) \\ x_{3d}(k+1) &= 1 + x_{2d}(k) - ax_{3d}^2(k). \end{aligned} \tag{5.44}$$

The response system is given by,

$$\begin{aligned} x_1(k+1) &= -bx_3(k) \\ x_2(k+1) &= x_1(k) + bx_3(k) \\ x_3(k+1) &= F(\boldsymbol{x}(k)) + u(k), \end{aligned} \tag{5.45}$$

or

$$\begin{bmatrix} x_1(k+1) \\ x_2(k+1) \\ x_3(k+1) \end{bmatrix} = \begin{bmatrix} 0 & 0 & -b \\ 1 & 0 & b \\ 0 & 0 & 0 \end{bmatrix} \begin{bmatrix} x_1(k) \\ x_2(k) \\ x_3(k) \end{bmatrix} + \begin{bmatrix} 0 \\ 0 \\ F(\boldsymbol{x}(k)) \end{bmatrix} + \begin{bmatrix} 0 \\ 0 \\ u(k) \end{bmatrix}, \tag{5.46}$$

where $a = 1.07$, $b = 0.3$, $F(\boldsymbol{x}(k)) = 1 + x_2(k) - ax_3^2(k)$ and $u(k)$ is the control signal.

In this simulation, initial conditions are chosen as $\boldsymbol{c} = [1 \quad 1 \quad 1]$, $\boldsymbol{x}_d(0) = [0.19 \quad 0.06 \quad 0.77]^T$ and $\boldsymbol{x}(0) = [-0.22 \quad 0.30 \quad -0.75]^T$. The chaotic attractor of $\boldsymbol{x}_d$ is shown in Fig. 5.3.3.

Denoting the error for input to FREN as $E = sign(e_3)\|\boldsymbol{x}_d - \boldsymbol{x}\|$, the fuzzy control rules are given by,

RULE 1 IF E IS PL THEN u IS PL
RULE 2 IF E IS PM THEN u IS PM
RULE 3 IF E IS NM THEN u IS NM
RULE 4 IF E IS NL THEN u IS NL.

The initial setting of membership functions and linear consequences of FREN are selected as shown in Fig. 5.17(a). After on-line learning, the final MF and LC of FREN become as shown in Fig. 5.17(b).

The trajectory of the drive system $\boldsymbol{x}_d$ and the response system $\boldsymbol{x}$ before and after learning phase are shown in Fig. 5.18 (a) and (b), respectively. The control effort and state parameters after learning phase are illustrated in Fig. 5.19.

The tests are performed by using RBFN and ANFIS and the results are summarized in Table 5.3.

Table 5.3: Comparisons of chaotic synchronization control algorithms.

Control algorithm	SSE_1	SSE_2	Training (epoches)
RBF[1:4:1]	Fail	-	5,000
RBF[1:50:1]	0.9274	-	2,000
ANFIS[1:20:1]	0.4017	2.9436	2,000
ANFIS[1:4:1]	0.8951	4.6837	2,000
FREN [1:4:1]	0.4162	2.0741	2,000

$SSE_1 = \sum_{i=1}^{3}\sum_{k=5}^{50} e_i^2(k)$, and $SSE_2 = \sum_{i=1}^{3}\sum_{k=1}^{60} e_i^2(k)$. Notice that SSE_2 includes the tracking error during the transient duration ($k = 1, 2, 3, 4$).

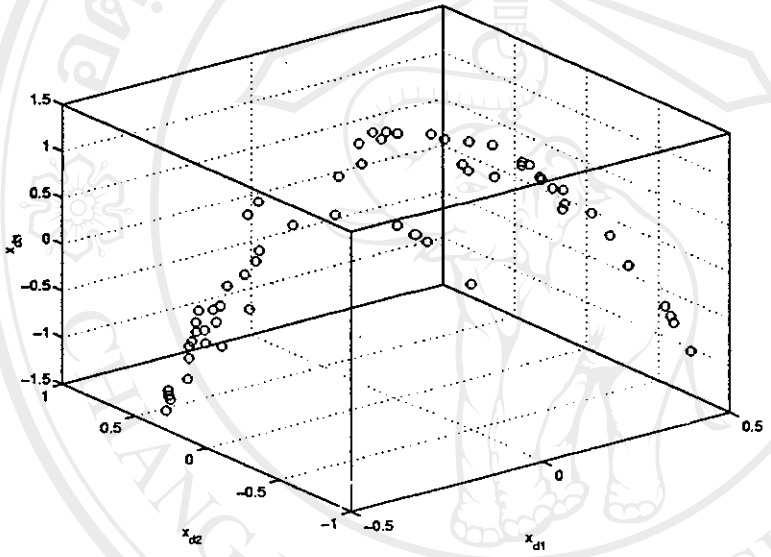

Figure 5.16: Generalized Hénon map.

It is found that RBF with 4 hidden nodes cannot make the response system synchronize with the drive system. The result from ANFIS with 20 hidden nodes is slightly better than FREN but the numbers of adjustable parameters and hidden nodes are around five times of FREN[1:4:1].

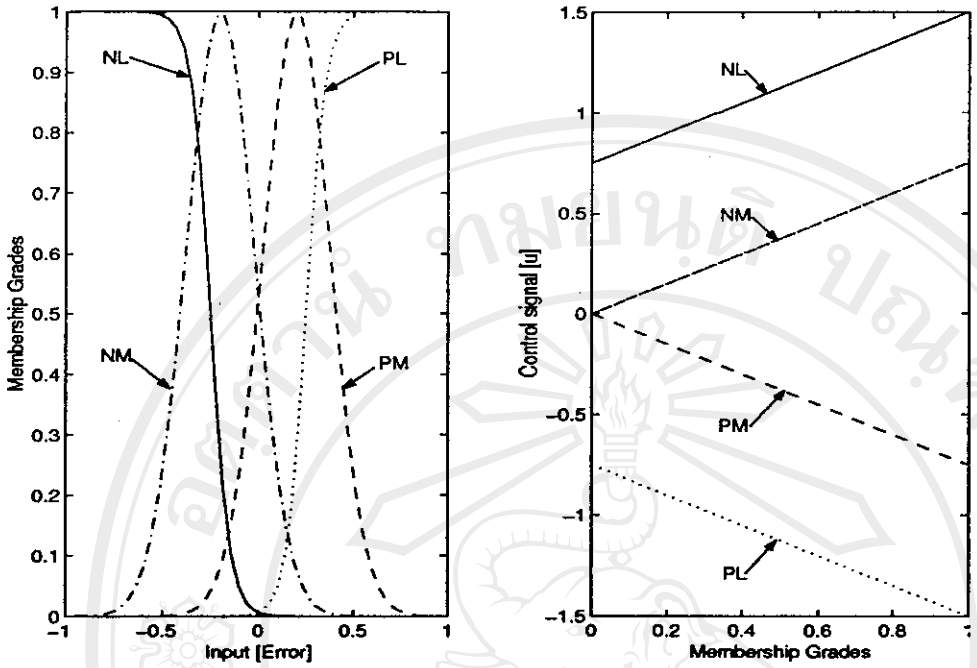

(a) Initial setting.

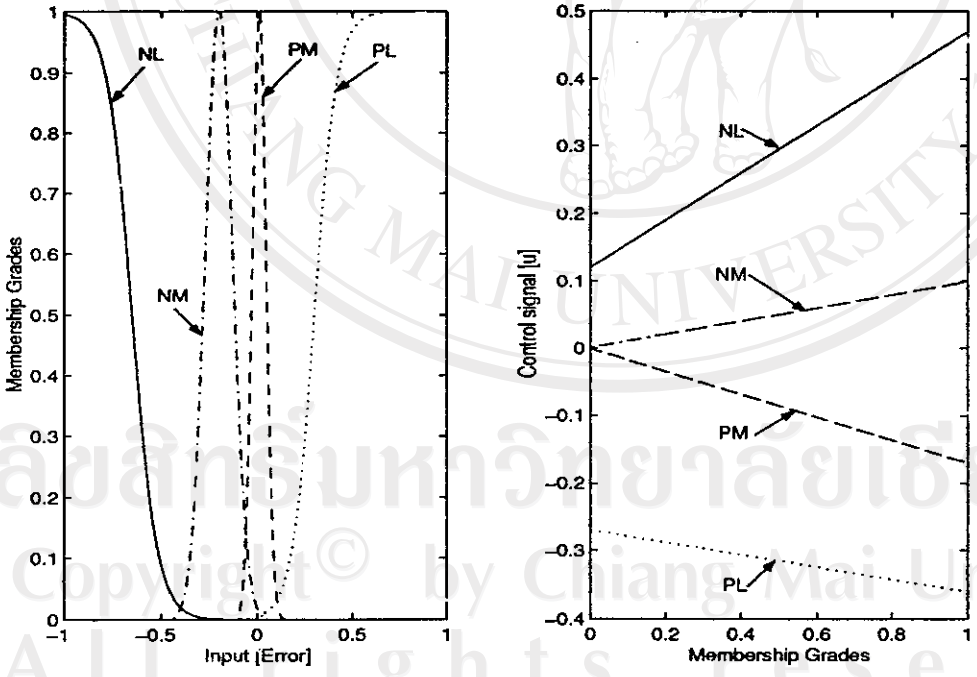

(b) Final setting.

Figure 5.17: MF and LC of Hénon map synchronization.

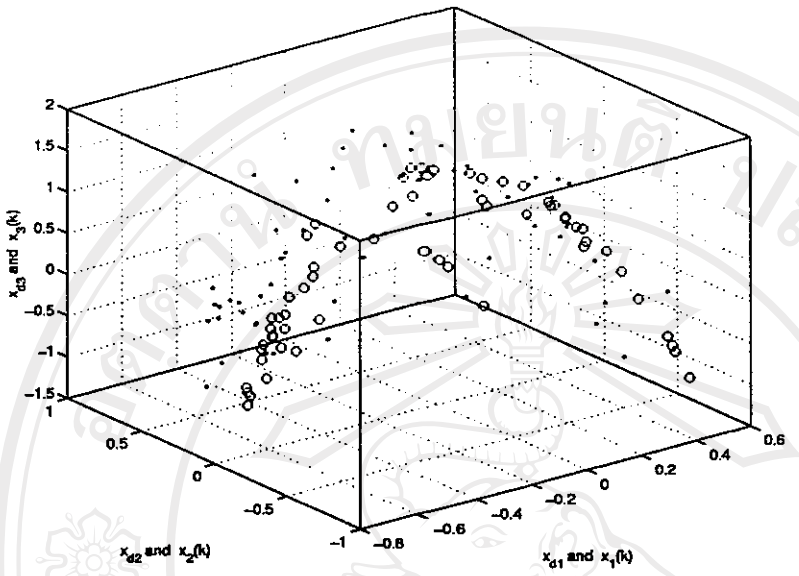

(a) Initial responses, $\circ \rightarrow \boldsymbol{x}_d$, $\bullet \rightarrow \boldsymbol{x}$.

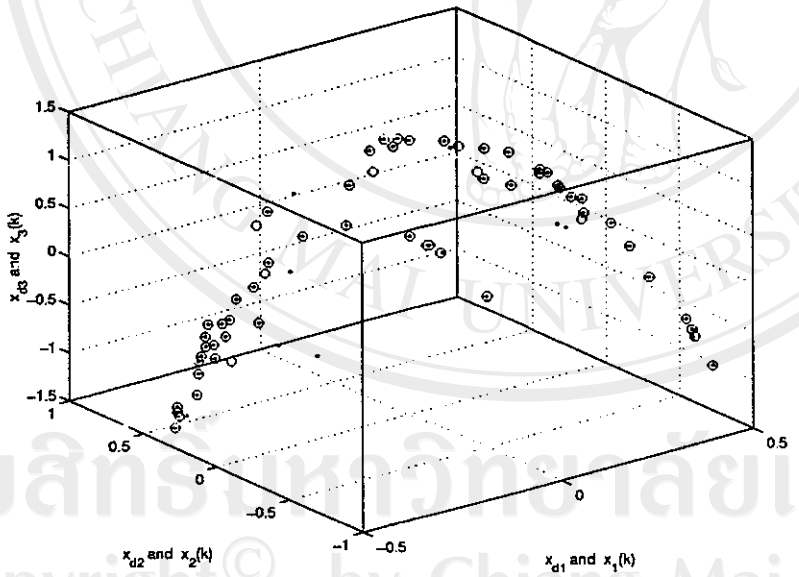

(b) Final responses, $\circ \rightarrow \boldsymbol{x}_d$, $\bullet \rightarrow \boldsymbol{x}$.

Figure 5.18: Initial and final results of Hénon map synchronization.

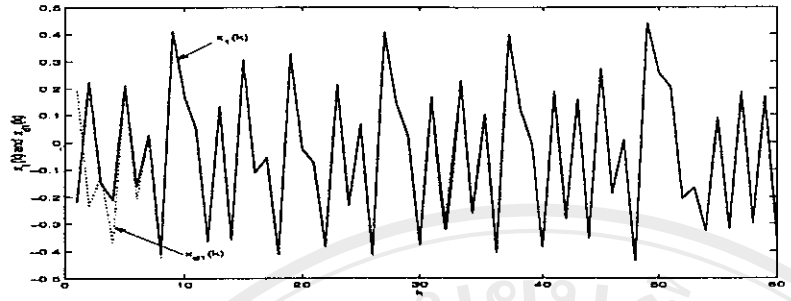

(a) $x_{d1}(k)$ and $x_1(k)$

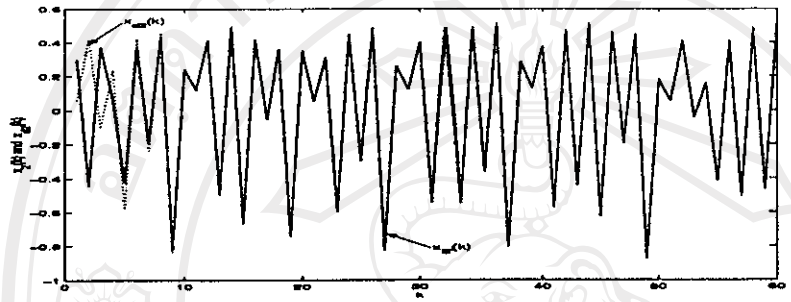

(b) $x_{d2}(k)$ and $x_2(k)$

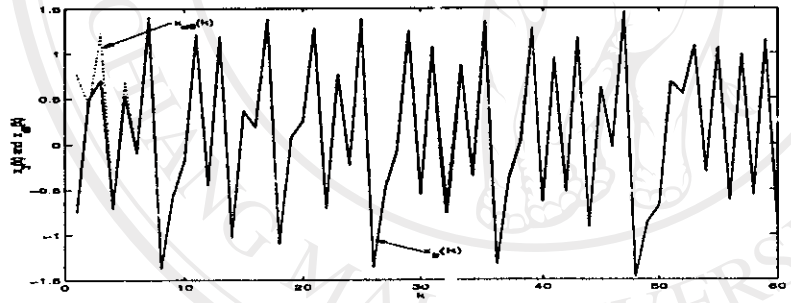

(c) $x_{d3}(k)$ and $x_3(k)$

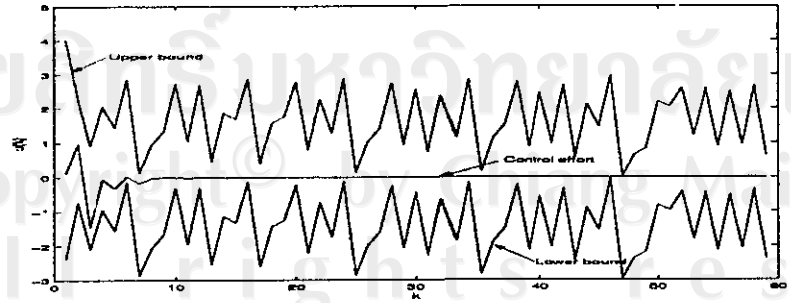

(d) control effort $u(k)$

Figure 5.19: State variables and control effort of Hénon map synchronization after learning phase.